On the global distribution of neutral gases in Titan's upper atmosphere and its effect on the thermal structure

I. C. F. Müller-Wodarg,[1,2,4] R. V. Yelle,[3] M. J. Mendillo,[2] and A. D. Aylward[1]

[1] Using a time-dependent general circulation model of Titan's thermosphere, we calculate the global distribution of neutral gases by winds and diffusion. Our calculations suggest that solar driven dynamics effectively redistribute constituents, causing considerable diurnal and seasonal changes in gas abundances. Subsidence causes an accumulation of lighter gases on the nightside, with nighttime CH_4 mole fractions at equinox near 1400 km reaching up to 50%. The reverse happens on the dayside, where lighter gases are depleted, giving minimum CH_4 mole fractions near 1400 km of around 12%. The vertical transport time scales are around 5–10% of a Titan day, so these extrema in gas abundances are shifted with respect to local noon and midnight by up to 4 hours Local Solar Time (LST). The strong horizontal variations in gas abundances, combined with the local time shifts of their extrema, have an important impact on the thermal structure and lead to a shift of the nighttime minimum from local midnight towards early morning hours (0330 LST). This coupling between gas distribution and thermal structure on the nightside occurs via dynamical processes, primarily through changes in adiabatic heating. The redistribution of gases effectively controls, through changes in mean molecular weight, the pressure gradients, which in turn control the horizontal and vertical winds, and thereby adiabatic heating and cooling. On the dayside, changes in solar EUV absorption due to the redistributed gases occur but are comparatively small. Although it is possible with our calculations to identify important processes, Voyager and ground based observations of Titan are currently not sufficient to constrain the dynamics of Titan's upper atmosphere, but comparisons with forthcoming Cassini observations are highly anticipated. *INDEX TERMS:* 6005 Planetology: Comets and Small Bodies: Atmospheres—composition and chemistry; 0355 Atmospheric Composition and Structure: Thermosphere—composition and chemistry; 3210 Mathematical Geophysics: Modeling; 6007 Planetology: Comets and Small Bodies: Atmospheres—structure and dynamics; 6025 Planetology: Comets and Small Bodies: Interactions with solar wind plasma and fields; *KEYWORDS:* Titan, thermosphere, composition, dynamics, temperature, modeling

Citation: Müller-Wodarg, I. C. F., R. V. Yelle, M. J. Mendillo, and A. D. Aylward, On the global distribution of neutral gases in Titan's upper atmosphere and its effect on the thermal structure, *J. Geophys. Res.*, *108*(A12), 1453, doi:10.1029/2003JA010054, 2003.

1. Introduction

[2] Saturn's largest moon Titan is in many respects extraordinary. A "terrestrial-type" body in the outer solar system, it possesses a thick atmosphere with surface pressure of 1.4 bars, comparable to that on Earth. Titan's atmosphere resembles that of Earth, furthermore, in that it is composed primarily of N_2, and a troposphere, strato-

sphere, mesosphere, and thermosphere can be recognized in the vertical thermal structure. The second most abundant gas on Titan is CH_4, followed by numerous hydrocarbons in smaller quantities. Being almost 10 times as far from the Sun as Earth, Titan's atmospheric temperatures are considerably lower, ranging from around 94 K near the surface to $\sim$175 K in the exosphere.

[3] Since the first comprehensive observations of Titan's atmosphere by the Voyager spacecraft in 1980, numerous theoretical studies and ground based measurements have been carried out, but many questions remain. For an overview of results from these studies, see *Müller-Wodarg et al.* [2000]. To date, no reliable observational constraints are available for dynamics and horizontal structure of temperature and composition in Titan's thermosphere. The forthcoming joint NASA/ESA/ASI Cassini/Huygens mission to Saturn and Titan will provide the opportunity to study Titan's atmosphere in unprecedented detail. In partic-

[1]Atmospheric Physics Laboratory, University College London, London, UK.
[2]Center for Space Physics, Boston University, Boston, Massachusetts, USA.
[3]Lunar and Planetary Lab, University of Arizona, Tucson, Arizona, USA.
[4]Now at Space and Atmospheric Physics Group, Imperial College, London, UK.
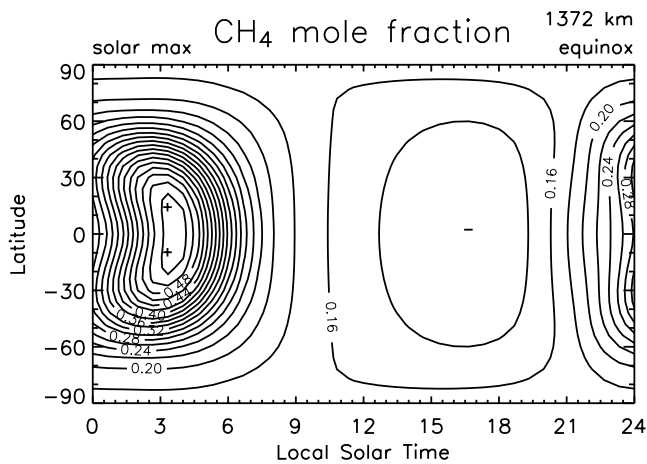
Figure 1. CH$_4$ mole fractions near the 1×10^{-3}nbar pressure level for equinox at solar maximum, as calculated by the Titan TGCM. The average height of the pressure level is 1372 km.

ular, the Cassini spacecraft on its orbits around Saturn will regularly dive into Titan's thermosphere down to around 950 km altitude and carry out in situ measurements of thermospheric composition and temperatures, thus determining horizontal and vertical structures of the region. A deeper theoretical understanding of Titan's global upper atmosphere is highly desireable in view of these forthcoming observations.

[4] Basic issues concerning the dynamics of Titan's thermosphere have previously been discussed by *Rishbeth et al.* [2000]. Using scale analysis of the equations of motion, they compared the dynamics of Titan's thermosphere with that on Earth and predicted some fundamental differences. *Müller-Wodarg et al.* [2000] and *Müller-Wodarg and Yelle* [2002] presented the first global calculations of temperatures and winds in Titan's thermosphere using a newly developed time-dependent Thermospheric General Circulation Model (TGCM). The same model is used for this study. The motivation for developing such a complex code is to gain a deeper theoretical understanding of the coupled dynamical, energetic, and composition response of Titan's thermosphere to external forcing, such as solar heating and magnetospheric particle flux from Saturn. In contrast to previous one-dimensional studies, these global simulations consider the effects of time-dependent solar input and horizontal coupling as well as self-consistent time-dependent dynamics.

[5] The basic equations solved by our TGCM have previously been presented by *Müller-Wodarg et al.* [2000] and, for the problem of three-component diffusion, by *Müller-Wodarg and Yelle* [2002]. For convenience, they are also given in Appendix A. The model solves self-consistently the three-dimensional (3-D) coupled equations of momentum, energy, and continuity by explicit time integration on pressure levels extending from 600 to ~1400 km altitude ($0.15-1 \times 10^{-6}$ μbar). It thereby calculates self-consistently the global response of Titan's upper atmosphere to time-dependent solar EUV heating, giving us theoretical predictions for global temperature profiles, winds and distribution of gases.

[6] Our first Titan TGCM calculations, as presented by *Müller-Wodarg et al.* [2000], suggested day-night temperature differences of up to 20 K, which drive horizontal winds of up to 60 m/s. The thermal structure and dynamical response was found to be strongly affected by the extended nature of Titan's thermosphere as well as strong curvature due to Titan's small radius. While the model originally in its calculations did not consider gas transport processes, it was recently extended to also solve the continuity equations for individual gases, thereby allowing for a separation of the gases by winds and diffusion. The implementation of these additional TGCM calculations was described by *Müller-Wodarg and Yelle* [2002]. They found that winds effectively mix constituents in Titan's thermosphere and could explain the large eddy coefficients of $(0.4-2.6) \times 10^9$ cm^2 s^{-1} between ~985 and 1125 km altitude which were inferred by *Strobel et al.* [1992] from the Voyager UVS observations.

[7] In the following, we extend the study by *Müller-Wodarg and Yelle* [2002] and discuss in more detail the wind-induced local time and seasonal distribution of gases in Titan's thermosphere and how this distribution affects the thermal structure. We use the same model as *Müller-Wodarg and Yelle* [2002] but carry out additional runs for different seasonal and solar conditions. Our calculations show a strong coupling among dynamics, energy, and composition on Titan, a result which may improve the constraints on dynamics posed by the anticipated Cassini observations. Winds will not be directly measured but can be inferred from composition and temperature observations.

[8] In section 2 we present Titan TGCM simulations for equinox and southern solstice conditions at solar maximum and discuss the physical implications in section 3. Conclusions will be given in section 4.

2. Results From Calculations
2.1. Diurnal and Seasonal Behavior

[9] Figures 1 and 2 show latitude-local time profiles of CH$_4$ mole fractions near the 1×10^{-3}nbar pressure level for equinox and southern hemisphere solstice conditions, respectively, at solar maximum. The chosen pressure level
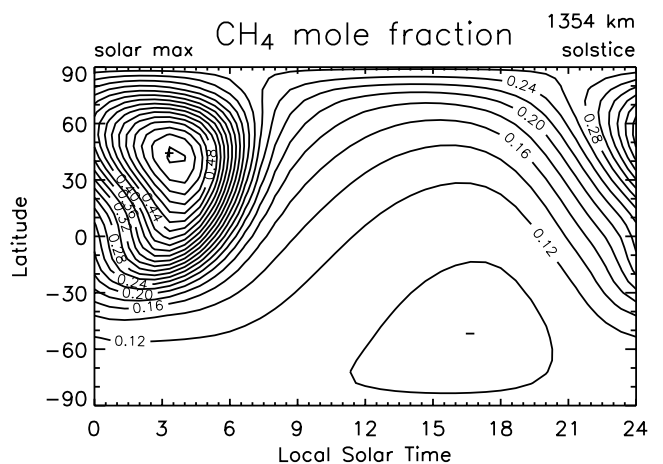
Figure 2. Same as Figure 1, but for solstice (southern summer) conditions. The average height of the pressure level is 1354 km.
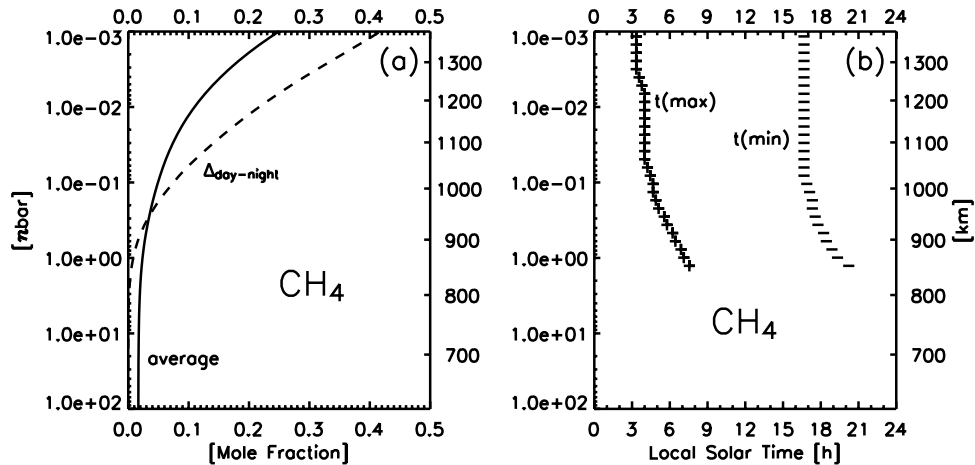
Figure 3. Daily averaged CH_4 mole fractions (a) (solid line) and maximum day-night differences (dashed line) as well as the local times of occurrence of the maxima and minima (b). The values are taken from the equinox simulation over the equator.

lies in the upper thermosphere at a globally averaged height of ~1372 km for the equinox case and ~1354 km for the solstice case. The equinox run (Figure 1) reproduces conditions encountered by the Voyager spacecraft in 1980/1981, while the solstice run (Figure 2) is roughly for conditions which the Cassini spacecraft will encounter upon its arrival at the Saturnian system in 2004. The most striking features in both panels are the substantial day-night differences and, for the solstice case, hemispheric differences in CH_4 abundances. Dayside (and summer) mole fractions are lower than nightside (and winter) values. At this particular pressure level daytime abundances of CH_4 reach around 12%, whereas nighttime peak values are near 54%. These extrema change to around 56% in the winter hemisphere and 9% in the summer hemisphere. At equinox, day-night differences are largest over the equator, while at solstice they are largest near 42° latitude in the winter hemisphere. Note that these substantial day-night differences in CH_4 abundance are driven entirely by dynamics and molecular diffusion, with no photochemistry being considered in our calculations, due to the long photolysis lifetimes of N_2 and CH_4 in Titan's thermosphere. The spacing of contour lines in Figures 1 and 2 shows that horizontal gradients are considerably larger on the nightside than on the dayside, with daytime abundances being nearly constant. The morphology behind these structures in composition will be examined further in section 2.2.

[10]   Figure 3 shows height profiles of daily averaged CH_4 mole fractions (Figure 3a, solid line) and the maximum day-night differences (Figure 3a, dashed line) as well as the local times of occurrence ("phases") of the maxima and minima (Figure 3b). The values are taken from the equinox simulation over the equator. Since day-night differences are negligible below around 850 km, the phase values (Figure 3b) are shown for higher altitudes only. The solid line in Figure 3a shows that daily averaged CH_4 abundances are roughly constant below 800 km and increase from the lower boundary value of 1.6% at 600 km to 25% near 1400 km. Maximum day-night differences (dashed line in Figure 3a) increase from zero below 900 km to around 0.4 at 1400 km. The phases of maxima and minima (Figure 3b)

are around 0320 and 1640 LST, respectively, at 1400 km and shift forward to around 0700 and 1830, respectively, near 900 km. The results suggest considerable day-night differences of CH_4 abundances in Titan's thermosphere induced by global-scale transport above around 1000 km altitude. According to our calculations, maximum CH_4 abundances occur in the early morning hours and minima during late afternoon hours. The causes for this behavior are further discussed in section 2.2.

[11]   With CH_4 being a thermally active constituent that absorbs solar EUV radiation, it is of interest to examine whether these transport-induced local time and seasonal changes affect temperatures as well. Figures 4 and 5 show latitude-local time profiles of neutral temperatures for the same pressure levels and seasonal conditions as Figures 1 and 2. Dayside temperatures are fairly constant, changing
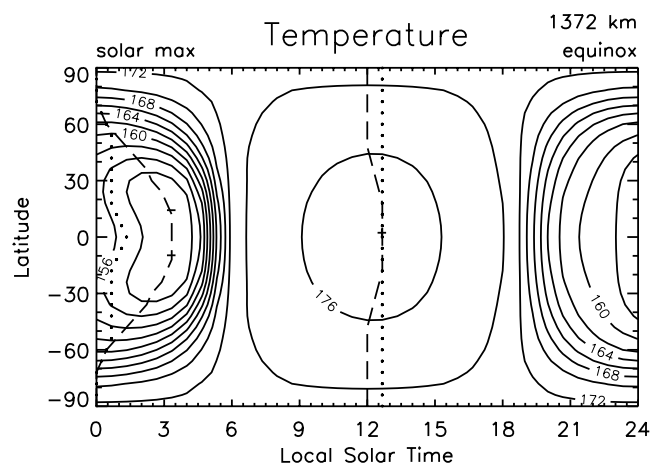
Figure 4. Latitude-local time profiles of neutral temperatures near the $1 \times 10^{-3} nbar$ pressure level for equinox at solar maximum, as calculated by the Titan TGCM. Dashed lines trace the local time extrema of temperature from this simulation, while dotted lines trace temperature extrema from a simulation for the same seasonal and solar conditions but with globally constant composition.
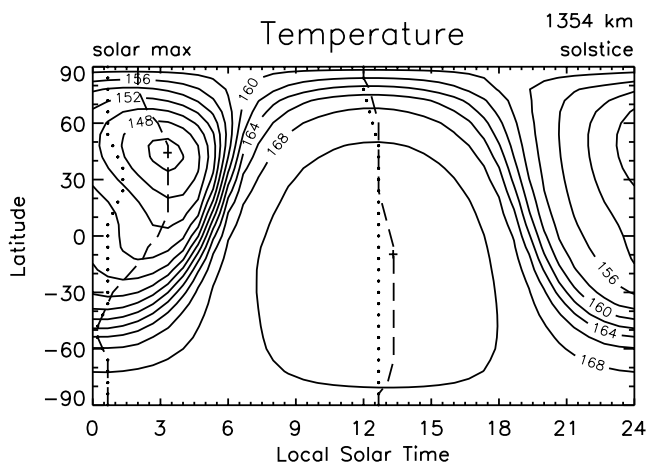
Figure 5. Same as Figure 4, but for southern hemisphere solstice.

by less than 4 K, but variations are larger on the nightside, falling by up to around 20 K. Similar behavior was found by *Müller-Wodarg et al.* [2000] and partly attributed to Titan's small size. With Titan's thermosphere considerably extended in space with respect to the solid body, the nighttime shadow cast by the optically thick part of Titan and its atmosphere near 1400 km only covers the region equatorward of around 60° latitude (under equinox conditions), so the higher latitudes are under continuous sunlight, even at night. Similarly, the local time behavior is affected, with the Sun "rising" up to 2 hours LST earlier and "setting" up to 2 hours later than 0600 LST and 1800 LST, respectively. Therefore the nighttime changes are concentrated in a smaller area of space, causing the gradients to be sharper. A reason for dayside temperatures to be fairly uniform in the upper thermosphere is the low optical thickness of the gases, implying that the local solar heating rate there is little dependent on the solar zenith angle.

[12] The dashed lines superimposed in Figures 4 and 5 mark the locations of the dayside maxima and nightside minima and illustrate that the local time of the dayside maximum occurrence is fairly constant with latitude, whereas that of the nighttime minimum changes considerably with latitude. Both at equinox and solstice the dayside maximum temperature occurs between 1200 and 1330 LST. At equinox, the minimum temperatures occur between midnight near the poles and 0330 LST near the equator, while at solstice the behavior is more complex and the local times of minimum temperature occurrence range from 0100 LST near the summer pole to 0330 in the winter hemisphere.

[13] In order to determine whether the temperature behavior is affected by composition changes shown in Figures 1 and 2, we compare our temperature profiles with those produced by simulations in which we assumed constant mixing ratios on each pressure level, ignoring gas transport by winds. These "fixed composition" simulations correspond in principle to those presented by *Müller-Wodarg et al.* [2000] but used a slightly different vertical composition profile. For best comparison with the "variable composition" runs, we used the globally averaged profiles of those runs and fed them into our "fixed composition" simulations to calculate temperatures and winds. We there-

by ensured that any differences between the two sets of simulations are entirely due to variations in composition. The largest day-night temperature differences on the pressure level of Figures 4 and 5 are around 25 K in the "variable composition" run and 20 K in the "fixed composition" run, irrespective of season, so allowing for the composition changes has increased the overall day-night temperature difference slightly.

[14] For a more detailed comparison of temperature behavior in the "variable composition" and "fixed composition" runs, we will also compare their phases. To do so, the local times of temperature maxima and minima from the "fixed composition" simulations are superimposed into Figures 4 and 5 as dots. In the following, we will compare the behavior of these "dots" with that of the dashed lines in Figures 4 and 5. The most striking difference between the "variable composition" and "fixed composition" runs at equinox is the location of the nightside minimum, which is shifted towards later local times by up to 2 hours LST. The differences between the dashed lines and dots in Figure 4 decrease towards the poles. At solstice (Figure 5) the differences in local time behavior are equivalent, but there is also a change of the latitudes of the summer temperature maximum and winter minimum. In the "fixed composition" runs the summer maximum and winter minimum are found to be located at the subsolar and antisolar points, respectively, near 24° latitude. In contrast, the maximum and minimum points in Figure 5 (marked by "+" and "−" in the contours) are located at 12° in the summer hemisphere and 42° in the winter hemisphere, respectively. So, the winter minimum has moved poleward and the summer maximum equatorward with respect to the "fixed composition" run.

[15] Figure 6 shows horizontal and vertical velocities for equinox on the same pressure level as Figure 4. Vertical velocities (contours) over the equator reach +0.58 m/s near 1040 LST and −0.72 m/s near 2100 LST. Horizontal winds blow essentially from day to night perpendicular to the isotherms (see Figure 4), reaching maximum velocities of
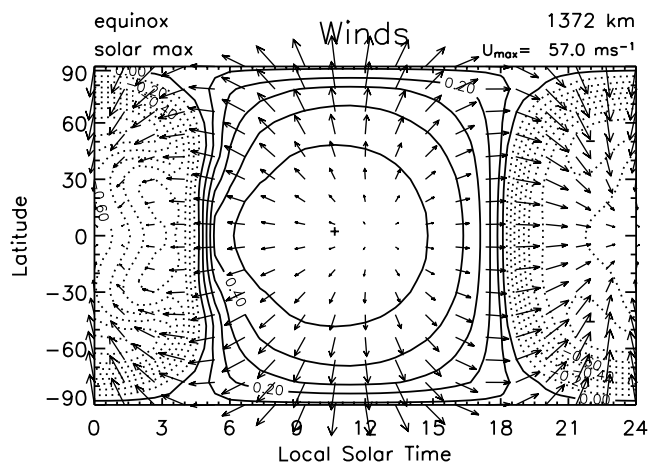
Figure 6. Latitude-local time profiles of horizontal and vertical winds near the 1×10^{-3} nbar pressure level for equinox at solar maximum, as calculated by the Titan TGCM. Vertical wind contour spacing is 0.1 m/s, the largest horizontal winds are 57 m/s.
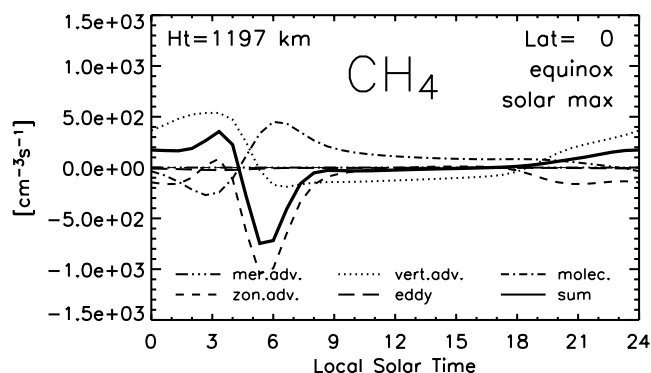
Figure 7. Terms of the CH_4 continuity equation over the equator at equinox versus local solar time.

around 57 m/s over the poles. Over the equator zonal winds are largest after sunset, near 1900 LST, reaching around 50 m/s. Note the asymmetries in vertical and horizontal winds in sectors from 0300 to 0900 LST and 1500 to 2100 LST. These asymmetries will be discussed further in section 4.3.

2.2. Daily and Seasonal CH_4 Flow

[16] In the previous section we described the local time and latitude variations in composition which are caused by solar driven dynamics and we showed how they affected the temperature behavior. In the following we will investigate what dynamical processes cause the transport and thereby the variations in constituent abundances. In doing so, we distinguish between the daily averaged interhemispheric flow which is largely controlled by the solar declination angle, or season, and the local time-dependent flow which is controlled by the solar hour angle, or Titan's rotation under the Sun.

[17] Figure 7 shows terms in the CH_4 continuity equation near 1200 km altitude over the equator at equinox versus local solar time. Averaged over a day, the total change is close to zero, but considerable local time variations are seen. The thick solid line is the sum of all terms, indicating a net inflow of CH_4 between 1800 and 0400 LST (positive values) and outflow at all other local times (negative values). During most of the daytime (0900–1800 LST) the net flow is close to zero, indicating almost constant dayside abundances, and most changes occur during nighttime. This behavior of flows is consistent with findings of Figure 1, which showed larger night than day abundances of CH_4 and almost constant dayside values. The flow of CH_4 in Figure 7 is driven primarily by vertical advection (dotted line), zonal advection (narrow dashed), and molecular diffusion (dashed-dotted). The particular choice of equatorial location and season implies that meridional flow (dashed-triple-dotted) is virtually zero, but this is not the case elsewhere, particularly at more poleward locations and during solstice. Eddy diffusion is negligible at this altitude in the atmosphere but becomes dominant below the homopause (near 1000 km on Titan).

[18] Vertical advection is driven by the divergence of horizontal winds on constant pressure surfaces and is upward during daytime and downward during night. Since CH_4 is the lighter gas in Titan's thermosphere, with a molecular weight smaller than the mean molecular weight,

it has a larger scale height than that of the total gas, so its mole fraction increases with altitude (see Figure 3a). Therefore upwelling on the dayside transports gas upward which originates from lower down and contains proportionally less CH_4, leading to a depletion of CH_4 there. The opposite happens on the nightside. Advection by zonal winds carries gas from hot to cold or day to night. They thus transport CH_4-depleted gas from the dayside to the nightside, acting as a CH_4 sink most of the time, particularly at dawn, where winds and, more importantly, horizontal composition gradients are strong. Molecular diffusion (dashed-dotted) mostly counteracts vertical advection, transporting CH_4, with the help of horizontal advection, into the dayside and out of the nightside. This describes the morphology behind the composition variations in Figures 1 and 2.

[19] Figure 8 shows diurnally averaged sources and sinks of CH_4 versus latitude for solstice (southern summer) conditions at solar maximum. The terms are plotted for the same pressure level as those in Figure 7. We see that vertical advection, zonal advection, and molecular diffusion again play an important role, but additionally meridional advection is important at solstice, acting mostly as a CH_4 sink. Vertical advection again plays a dominant role, feeding CH_4 into the winter hemisphere and reducing it in the summer hemisphere. Interestingly, zonal flow is very important too, depleting the winter hemisphere of CH_4. Flows are generally weaker in the summer hemisphere, correlating well with the relatively invariant summer hemisphere temperatures (Figure 5), which drive smaller winds.

[20] The diurnal (Figure 7) and seasonal (Figure 8) flow of gases can be explained by the presence of two large circulation cells in the atmosphere, the diurnal (zonal) cell and the meridional (interhemispheric) cell. Interhemispheric flow is created primarily at solstice by the asymmetric heating of the two hemispheres. Although there is also a meridional flow present at equinox, we found its daily averaged values to be at least an order of magnitude smaller than values at solstice. So, at equinox the variations in CH_4 abundance are primarily with local time, only on the nightside there are some latitudinal variations due to Titan's high-latitude nightside heating. Gases are transported up on the dayside, leading to a reduction in light gas abundances
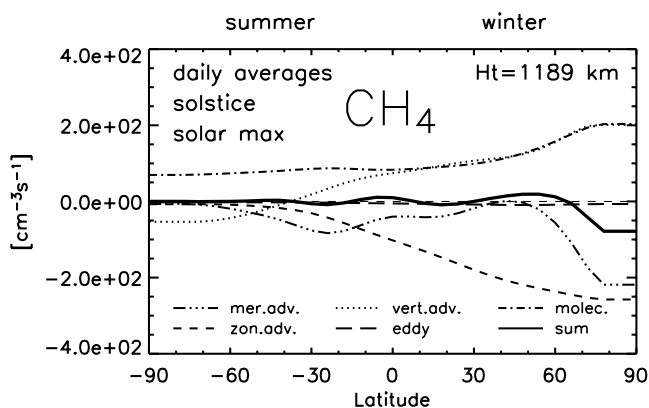
Figure 8. Diurnally averaged terms of the CH_4 continuity equation versus latitude for solstice (southern summer) conditions at solar maximum, as calculated by the Titan TGCM.

(CH$_4$), and down on the nightside, enhancing the light gas abundances. A zonal flow at dawn and dusk closes the circulation cell. Note that the vertical flow plotted in Figures 7 and 8 is not caused by the thermal expansion and contraction of the atmosphere but is a result of vertical divergence winds which transport gases relative to pressure levels. Both Figures 7 and 8 are plotted on a fixed pressure level rather than altitude in order to clearly separate the divergence winds and their transport from the vertical gas transport due to barometric (thermal expansion) winds. At solstice, an additional circulation cell is set up by the uneven heating of the hemispheres. Summer upwelling reduces the light gas abundances there; winter downwelling causes the opposite. Horizontal flow again closes the interhemispheric circulation cell. Meridional winds blow from summer to winter, transporting gases from the (CH$_4$ deprived) summer into the (CH$_4$ rich) winter hemisphere (hence acting as a net sink of CH$_4$), slightly offsetting the abundance gradients set up by vertical winds. The diurnally averaged meridional summer-to-winter winds in our simulations reach around 10 m/s at low to middle latitudes. Owing to the action of Coriolis forces, this meridional flow also generates a net zonal flow with a maximum near 40° latitude, being eastward in the winter and westward in the summer hemisphere with peak winds of around 5 m/s. So, the interhemispheric flow not only creates a net meridional transport but also a net zonal one (narrow-dashed curve in Figure 8). Although the zonal winds are smaller than the net meridional winds, zonal gradients in CH$_4$ are larger than the meridional gradients, so the two flows are comparable in Figure 8.

[21] The above terms analysis has shown not only what causes the composition structure of Figures 1 and 2 but also how important both vertical transport (through vertical advection and molecular diffusion) and horizontal transport (through horizontal advection) are. It is a striking demonstration of the need to study Titan's thermosphere in 3-D.

2.3.   Comparison of Dawn and Dusk Sectors

[22] Our results so far show global structures of CH$_4$ mole fractions and temperatures in Titan's thermosphere and suggest that the two influenced each other. With N$_2$ and CH$_4$ being the main absorbers of solar EUV radiation in Titan's thermosphere, it is of interest to investigate how far composition changes affect the solar EUV heating rates. We investigate this by comparing the dawn (LST = 0600) and dusk (LST = 1800) sectors.

[23] Figure 9 shows vertical profiles of dusk/dawn ratios of N$_2$ and CH$_4$ number densities (dashed), as well as EUV volume heating rates (solid). The values are for equinox and solar maximum conditions over the equator. CH$_4$ dusk/dawn ratios are below 1 at all heights, while the N$_2$ ratios are larger than 1 everywhere, indicating that CH$_4$ mole fractions are larger at dawn than dusk, while the opposite happens with N$_2$, as expected. This behavior of CH$_4$ is also evident from Figure 1 by comparing the values at 0600 LST ("dawn") with those at 1800 LST ("dusk") over the equator. The smallest CH$_4$ dusk/dawn ratio is around 0.3 near 1000 km (0.1 $n$bar), while the N$_2$ ratio reaches 1.3 near 1400 km, the top of the model range. In the following, we relate these dusk/dawn composition ratios to differences in EUV heating rates.
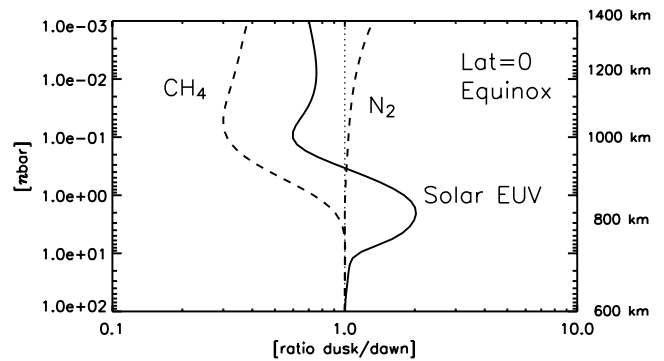
Figure 9.   Vertical profiles of dusk/dawn ratios of N$_2$ and CH$_4$ number densities (dashed). Also shown are dusk/dawn ratios of EUV volume heating rates (solid). All values are for equinox/solar maximum conditions over the equator.

[24] The solid curve in Figure 9 shows that the dusk/dawn ratios of EUV volume heating rates are larger than unity below around 900 km and less than unity at higher altitudes. Dusk/dawn ratios of heating rates reach around 2.0 near 820 km and 0.6 near 1000 km. Comparing this with the composition ratios from above, it appears that the larger dawn EUV heating rates above 900 km are a result of the higher dawn abundances of CH$_4$, while the behavior of the heating rates appears less correlated with local composition changes at lower altitudes.

[25] *Müller-Wodarg et al.* [2000] presented a vertical profile of EUV volume heating rates in Titan's thermosphere and pointed out a double-peak structure, in which the lower peak (near 750 km, or 1 $n$bar) was caused primarily by the Lyman α (1216 Å) line absorption and the upper peak (near 1000 km, or 0.1 $n$bar) by other solar EUV emissions. Only CH$_4$ absorbs the bright solar Lyman α line, and the CH$_4$ distribution affects the solar heating rate far more than the distribution of N$_2$. Therefore the distribution of CH$_4$ is expected to affect solar EUV heating rate far more than the distribution of N$_2$. This is indeed confirmed by results in Figure 9. Nevertheless, the differences in solar EUV heating rates at dawn and dusk, in spite of large differences in composition, do not appear to be very substantial, partly because changes in gas abundances will to first approximation only affect the height distribution of photon absorption not the column-integrated heating rates.

[26] Interestingly, the dusk/dawn EUV heating ratio becomes larger than 1 below around 900 km, indicating smaller heating rates at dawn than dusk, opposite to the trend above. This behavior is not correlated with composition changes in the same height range. Instead, what causes this behavior is that the stronger dawn EUV absorption above 900 km (due to higher abundances of CH$_4$) absorbs an important part of the solar energy, so the atmosphere becomes more optically thick at dawn and less EUV energy penetrates below 900 km. Therefore the dawn heating below 900 km is smaller than that at dusk, even though the local composition changes suggest no such trend. This is an example of how the thermosphere above influences regions below by changing its degree of opacity at EUV wavelengths. In the following section we will discuss what effects these composition-induced changes in

Table 1. Time Constants in Titan's Thermosphere for Eddy Diffusion (τ_K), Molecular Diffusion (τ_D), Horizontal Winds (τ_U), and Vertical Winds (τ_w), Based on Calculations by the Titan TGCM for Equinox Conditions at Solar Maximum[a]

Ht, km	τ_K, h	τ_D, h	τ_U, h	τ_w, h
600	100	10^5	10^5	10^5
800	100	100	10^3	10^3
1000	100	10	100	100
1200	100	1	10	10
1400	100	0.1	10	10

[a]All times are given in hours. For reference, the length of a Titan day is ~400 hours.

EUV heating rates have on the local time behavior of Titan's thermospheric temperatures.

3. Composition Structure

[27] Our previous discussions showed that winds play a key role in redistributing constituents in Titan's thermosphere. In the following, we will compare the transport time scales of horizontal and vertical winds with those of molecular and eddy diffusion, thereby gaining a deeper understanding of their relative importance and of the resulting CH_4 distributions, in particular with regards to the phases of CH_4 maxima and minima discussed earlier. Table 1 shows time scales for eddy diffusion (τ_K), molecular diffusion (τ_D), horizontal winds (τ_U), and vertical winds (τ_w) in Titan's thermosphere for solar maximum conditions. These time scales are given by $\tau_U = R/U$, $\tau_w = H/w$, $\tau_K = H^2/K$, and $\tau_D = H^2/D_{ij}$, where R is the radius of the planet, U is the horizontal neutral wind velocity, w is the vertical divergence velocity, H is the scale height, K is the eddy diffusion coefficient due to small scale turbulence, and D_{ij} is the molecular diffusion coefficient between gases i and j. Currently, there are no observational constraints for the value of K; in the Titan TGCM we assume $K = 5 \times 10^7$ cm^2/s. The numerical values in Table 1 were calculated using these expressions and parameter values (in particular wind speeds) from the Titan TGCM. In general, the shortest time scale in each height regime indicates the dominant gas transport process. On the basis of dynamical time scales we may distinguish between three main height regimes in Titan's thermosphere. Below 800 km ("Region A"), eddy diffusion is dominant, gases are uniformly mixed, and their relative abundances constant with height. This is confirmed by the vertical profile of average CH_4 abundances in Figure 3a (solid line). The eddy diffusion time scale is $\tau_K \sim 100$ h, which is comparable to the duration of a Titan day (~400 h), while all other time scales are 3 orders of magnitude longer. Between 800 and 1200 km altitude ("Region B"), time scales for vertical and horizontal wind transport (τ_w, τ_U) are comparable to those of molecular diffusion (τ_D), while above 1200 km ("Region C") molecular diffusion becomes dominant, so constituents increasingly distribute vertically according to their scale heights.

[28] Without the influence of winds, the gases in Regions B and C would distribute vertically according to their individual scale heights and any horizontal structure would be that imposed from below, the boundary to Region A, on which Regions B and C "sit." However, the dayside heating in Titan's thermosphere does generate vertical and horizontal winds which disturb this diffusive balance distribution. Molecular diffusion acts to restore the balanced distribution, in a manner that it depends on the relative time scales of winds and molecular diffusion in how far the resulting profile departs from the balanced distribution. In Region B, both time scales are of similar order, whereas in Region C molecular diffusion is quicker. Therefore the departure from the balance distribution is largest in Region B, whereas in Region C, in spite of strong winds, molecular diffusion is quick enough to restore balance. Since Region C "sits" on Region B, the horizontal distribution in Region C is that of the boundary between both regions. So, although diffusive balance is restored vertically in Region C, there is still horizontal structure in the form of strong diurnal changes in CH_4 mixing ratios. The strong local time changes are seen also above 1200 km altitude due to the boundary conditions imposed by Region B.

[29] Some uncertainty remains with regards to the latitudinal distribution of constituents. While we may safely ignore chemistry when examining diurnal changes, it may need to be considered when looking at hemispheric structures, particularly during solstice. Parts of the high-latitude winter thermosphere are in continuous darkness during solstice for many years, enough for chemical time scales to potentially play a role. The relative contributions of transport and chemistry to the seasonal distribution of constituents in Titan's stratosphere was investigated by *Lebonnois et al.* [2001]. Their calculations suggested vertical and horizontal transport to control the latitudinal gradients, while chemistry controlled mean concentrations. The question will be addressed for the thermosphere in future studies.

[30] By examining the transport time scales, we can also understand the phases of CH_4 maxima and minima. As outlined earlier, an increase in CH_4 mixing ratio is caused by downwelling, or downward vertical divergence winds, w, relative to the pressure levels. Therefore the phases of CH_4 should be correlated with those of w. CH_4 phases are shown in Figure 3b. Above 1000 km, the daily CH_4 maximum over the equator occurs between 0330 and 0500 LST and the minimum near 1640 LST. In the same locations, vertical wind phases (not shown) are 1130 LST (maximum upward) and 2130 LST (maximum downward). So, there is a phase shift between the vertical winds and CH_4 abundances of 4 hours LST on the dayside and 6 hours on the nightside. These values are comparable in magnitude to the vertical wind transport time scales in Table 1. At lower altitudes, CH_4 phases shift towards later local times by several hours (see Figure 3b), whereas vertical wind phases (not shown) remain fairly constant with altitude in the thermosphere. However, transport time scales become longer lower down in the atmosphere, so CH_4 "lags behind" even more. The diurnal amplitude and phase behavior of Figure 3 can thus be understood on the basis of vertical wind transport time scales.

[31] Titan's thermosphere is special in that its vertical wind transport time scale is ~5–10% of a local day, whereas on Earth at low to middle latitudes it is ~50–80% of a local day and on Venus ≪ 1% of a local solar day. So, transport introduces a phase lag between the vertical winds (and thus thermal structure) on Titan and composition. On Earth, long vertical transport time scales imply that
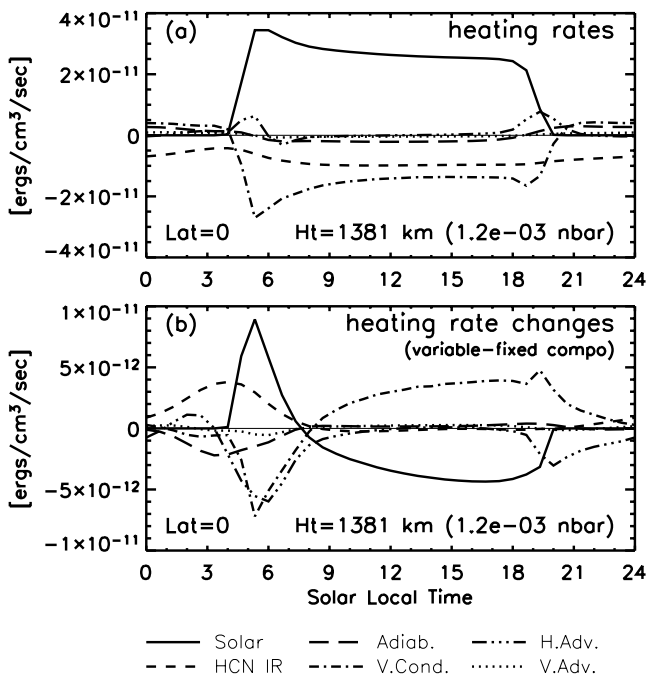
Figure 10. Heating and cooling rates over the equator near 1380 km altitude for equinox conditions at solar maximum. (a) The rates from the "variable composition" run, and (b) the differences between the "variable composition" and "fixed composition" simulation.

diurnal composition changes are very small, whereas on Venus the slow rotation implies that composition extrema are strong and well aligned with the thermal structure extrema. Therefore Titan can in this respect be regarded as a case between Venus and Earth. In terms of relative abundances we may compare CH_4 on Titan with O or He on Earth and O on Venus. These are minor gases in the lower thermospheres of each planet and become dominant in the upper thermospheres. The behavior of O mixing ratios in the Earth's thermosphere is somewhat different from that of CH_4 on Titan in that diurnal changes are considerably less and maximum O abundances occur near 0900 LT *Rishbeth and Müller-Wodarg* [1999], rather than at 0330 LST like on Titan. This difference is in part a result of Earth's faster rotation rate. Calculations by *Bougher et al.* [1999] suggested abundances of O on Venus to peak at local midnight and be smallest at local noon. The missing phase shift on Venus is a result of its slow rotation rate, which also causes diurnal variations in O to be large, as on Titan. In section 4.3 we will show that this composition phase shift on Titan has an important influence on the temperature structure.

4. Coupling Between Composition and Temperatures

4.1. Heating and Cooling Processes

[32] Figure 10 shows heating and cooling rates over the equator near 1380 km altitude for equinox conditions at solar maximum. We chose this particular pressure level for consistency with Figure 4 but found that terms behave qualitatively the same lower down in the atmosphere, near the $\tau = 1$ level at $\approx$1000 km. Figure 10a shows the rates

from the "variable composition" run, while in Figure 10b values are the differences between the "variable composition" and "fixed composition" simulation, so a positive (negative) value in any curve in Figure 10b implies a larger (smaller) value of that parameter in the "variable composition" simulation. For a heating process, a positive value in Figure 10b implies stronger heating in the "variable composition" simulation; for a cooling process a positive value implies weaker cooling. The opposite applies to negative values. Therefore the interpretation of values in Figure 10b is rather complex and can only properly be done with the information contained in Figure 10a.

[33] It is obvious from Figure 10a that solar EUV heating (solid line) in Titan's upper thermosphere is balanced mainly by vertical conduction (dashed-dotted) and HCN IR cooling (narrow-dashed), in agreement with earlier findings by *Müller-Wodarg et al.* [2000]. On the nightside, the energy balance is between HCN IR cooling, vertical conduction (dashed-dotted), and adiabatic heating (wide-dashed). Adiabatic heating during nighttime and cooling during daytime reduce the day-night temperature difference and horizontal advection (dashed-triple-dotted) transports energy into the dawn and dusk sectors.

4.2. Changes in EUV Heating and IR Cooling

[34] From Figure 10b it is evident that solar EUV heating (solid curve in Figure 10b) is larger by up to 25% in the "variable composition" run at dawn (0400–0730 LST) and smaller by around 15% during daytime (0900–2000 LST), with respect to the "fixed composition" case. This behavior is due to changes in CH_4 abundances in the "variable composition" run and was already discussed in section 2.3. As shown in Figure 1, CH_4 mole fractions are enhanced on the nightside and reduced on the dayside. As a result, solar EUV radiation incident upon the atmosphere at dawn encounters an atmosphere rich in CH_4, which leads to more efficient absorption of energy at dawn, and thereby larger heating rates. Throughout the day, CH_4 abundances are reduced (as a result of upwelling from the CH_4-poor lower atmosphere), and thereby the ability to absorb EUV radiation at that pressure level is reduced as well. So, the behavior of the EUV heating curve in the "variable" and "fixed" composition simulations is a direct result of changes in CH_4 abundances. A similar correlation exists for the infrared cooling rates (narrow-dashed) and HCN abundances. Being a heavier gas than CH_4, HCN is enhanced during the daytime and reduced during nighttime. Our simulations (not shown) predict an equatorial mixing ratio of 9×10^{-4} near 0400 LST and $\sim$16 $\times 10^{-4}$ between 1100 and 1800 LST near 1380 km. As a result HCN IR cooling rates are lower between 0000 and 0800 LST in the "variable composition" run, as shown by the positive values of the narrow-dashed curve in Figure 10b.

[35] *Lebonnois et al.* [2003] investigated the impact of seasonal composition changes in Titan's stratosphere on the temperature structure. In their study, the hemispheric temperature structure was affected by composition through changes in infrared cooling rates due to variations in the abundances of radiatively active gases such as C_2H_6, C_2H_2, and HCN. Although their study looked at a different region of the atmosphere where thermal structure is controlled by different processes, the parallel is that HCN cooling also

plays an important part in the thermosphere. However, the dynamically induced variations in HCN abundances and cooling rates in Titan's thermosphere appear to be relatively insignificant and hardly affect the resulting temperatures. The same applies to hemispheric differences in HCN abundances during solstice. Although more HCN is found in the summer hemisphere, the resulting increase in summer hemisphere IR cooling is far smaller than hemispheric differences in EUV heating or vertical conduction.

[36] So far we have discussed how wind-induced changes of gas abundances affected solar EUV heating and IR cooling rates. Our results explain the slight shift of the daytime temperature maximum towards earlier local times (see Figure 4), but they do not account for the most striking change, the pronounced nightside temperature minimum and its offset from the antisolar point. Clearly, EUV absorption is irrelevant on the nightside, and HCN cooling cannot explain the changes to the nightside temperature structure.

4.3. Dynamical Heating and Cooling

[37] In the following, we will discuss the importance of two internal energy redistribution processes, adiabatic heating and advection. We will show that these processes determine the nightside temperature behavior in Titan's thermosphere.

[38] Figure 10a shows that adiabatic heating, horizontal advection, and HCN IR cooling are the main process regulating the thermal structure on the nightside. In our "fixed composition" simulations (not shown here) all three of these processes act symmetrically around local midnight, making the temperatures symmetric as well, with the minimum at midnight. In our "variable composition" runs (Figure 10a) this is not the case. Adiabatic heating is considerably larger in the premidnight than postmidnight sector. This causes the temperature asymmetry around local midnight seen in Figures 4 and 5. Although horizontal advection heating rates also play a role, they are still far more symmetric around midnight than the adiabatic heating rates. Therefore they make only a second order contribution towards the asymmetry.

[39] Adiabatic processes are coupled to composition via the horizontal and vertical winds. Horizontal gradients in mean molecular weight affect the horizontal pressure gradients, which in turn drive horizontal winds. These, in turn, affect vertical winds to conserve mass, and vertical winds control adiabatic heating and cooling. This can also be seen in our simulations. The reason for adiabatic heating to be reduced in the dawn sector lies in the vertical winds there being lower as well. In the "fixed composition" runs equatorial vertical winds during equinox and solar maximum conditions near 1380 km altitude reach around −1.3 m/s both at 0300 and 2100 LST. In contrast, they reach −0.3 m/s and −0.7 m/s, respectively, in the "variable composition" runs (see Figure 6). Vertical divergence winds are caused by diverging horizontal winds, so these asymmetries in the predawn and postdusk sector vertical winds must be matched in the horizontal winds. In fact, zonal winds at the same locations in our "variable composition" simulation reach 20 m/s (westward) in the predawn sector and 35 m/s (eastward) in the dusk sector (Figure 6). Zonal winds, thereby, are weaker in the predawn than postdusk
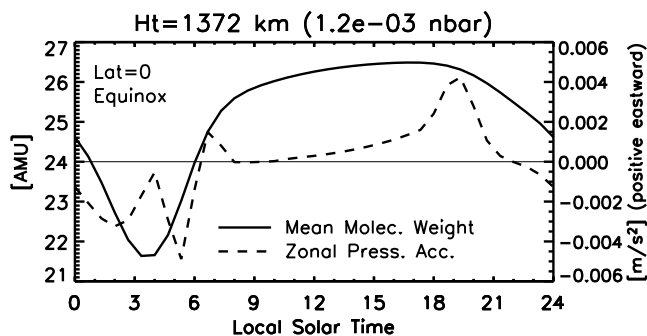
Figure 11. Mean molecular weight (solid) and zonal pressure gradient acceleration (dashed) over the equator near 1380 km altitude for equinox conditions at solar maximum.

sector. The same applies to meridional winds, as can be seen in Figure 6, and reduces the horizontal wind divergence in the predawn sector.

[40] Horizontal neutral winds, in turn, are driven by pressure gradients in the atmosphere. Figure 11 shows mean molecular mass (solid) and acceleration due to the zonal pressure gradient (dashed line, positive eastward) over the equator near 1380 km altitude for equinox conditions at solar maximum. The zonal pressure acceleration is eastward during most of the day, peaking near 1900 LST, and westward between 2100 LST and 0600 LST. It is clear from the behavior of the dashed curve in Figure 11 that the near-dawn (0300–0900 LST) and near-dusk (1500–2100 LST) sectors are not symmetrical. Westward acceleration is clearly weaker between 0200 and 0530 LST. This may at first seem surprising, given the stronger temperature gradients there. The reduction in zonal pressure acceleration however coincides with a minimum in mean molecular mass (solid curve), and we will show in the following that the two are strongly coupled.

[41] Horizontal accelerations are driven by pressure gradients, which themselves are equivalent to gradients in the height of a fixed pressure level which, to a first approximation, may be regarded as gradients in scale height. The scale height may be expressed as $H = kT/(mg)$, where k is the Boltzmann constant, T is the temperature, m is the mean molecular weight, and g is gravity, so horizontal gradients in scale height H, and thereby in pressure, are affected by horizontal gradients in mean molecular weight. Thus the key in reducing predawn sector horizontal pressure gradients lies in the behavior of mean molecular weight. Although the nightside is colder than the dayside, it also has a higher abundance in CH_4 (see Figures 1 and 2), and thus has a lower mean molecular weight. As seen from the solid curve in Figure 11, values of m near 1400 km reach 21.4 near 0300 LST and 26.5 near 1700 LST.

[42] Another important factor in creating this asymmetry are the transport time scales in Titan's thermosphere. As shown in Table 1 and discussed in section 3, vertical transport time scales are ∼5−10% of a local day. As a result, the changes in wind-induced composition need a few hours to react. So, although vertical winds are downward after sunset, enhancing the proportion of light gases (CH_4) and reducing the mean molecular weight, the impact of this

downwelling is strongest in the early morning hours, with lowest mean molecular weight values occurring near 0400 LST, just before sunrise. Similarly, the dayside maximum of m is shifted with respect to local noon, at around 1700 LST. Dayside values of m are more uniform than the nightside ones which is due, in part, to the more uniform dayside temperatures, discussed in section 2.1.

[43] With mean molecular weight changing as substantially with local time as shown in Figure 11, it is of interest to investigate also the diurnal behavior of scale height. While mean molecular weight was found to be lowest near 0400 LST, this is also the time of lowest temperatures, so the extrema of scale height do not coincide with those of either mean molecular weight or temperature. Near 1300 km we find scale height over the equator at equinox to vary from 88 km near 2100 LST to 104 km near 0600 LST. At solstice, diurnal variations of scale height are largest in the winter hemisphere near 18° latitude, ranging for $\approx$1300 km altitude from 83 km at 2100 LST to 95 km at 0600 LST.

5. Conclusions

[44] Our simulations have shown that dynamics, temperature and composition are strongly coupled on Titan. Our key findings are that (1) there exists a pronounced asymmetry in the local time behavior of temperature which (2) is caused by the strong dynamically induced local time changes in composition, affecting horizontal pressure gradients and adiabatic heating. A necessary condition for this asymmetry to occur is that (3) transport time scales of gases in Titan's thermosphere are around 10% of a day. This complex link between composition and temperature via dynamical processes is particularly pronounced on Titan and in part also a result of its slow rotation rate, combined with the curved geometry. The strength and nature of this coupling is thus unique on Titan.

[45] While our simulations are physically self-consistent, we cannot currently constrain them with any reliable measurements. As discussed already by *Müller-Wodarg et al.* [2000] and *Müller-Wodarg and Yelle* [2002], other factors may affect the wind profiles on Titan, such as magnetospheric heating through precipitating electrons from Saturn's magnetosphere and coupling to the lower atmosphere through upward propagating waves or zonal jets. Our simulations will provide an important comparison with forthcoming observations by the Cassini spacecraft and contribute towards maximizing the yield from observations by adding to our understanding of the complex coupled processes which determine spatial and temporal changes. Still, the basic physical effects discovered here should apply for a wide range of boundary conditions on Titan's thermosphere. Our predicted changes in neutral composition will also affect the diurnal and seasonal structure of Titan's ionosphere. The implementation of self-consistent calculations of Titan's coupled thermosphere and ionosphere in our model is planned for the near future.

Appendix A

[46] The Titan TGCM solves numerically by explicit time integration the coupled three-dimensional (3-D) Navier-Stokes equations of momentum, energy and continuity.

The two horizontal components of the momentum equation may in spherical pressure coordinates be expressed as

$$\frac{\partial u_\theta}{\partial t} = -\left(u_\theta \frac{1}{a}\frac{\partial u_\theta}{\partial \theta} + u_\varphi \frac{1}{a\cdot\sin\theta}\frac{\partial u_\theta}{\partial\varphi} + w\frac{\partial u_\theta}{\partial p}\right) + \left(\frac{-wu_\theta}{a} + \frac{u_\varphi^2}{a\cdot\tan\theta}\right)$$

$$-\frac{g}{a}\frac{\partial h_p}{\partial\theta} + 2\Omega u_\varphi \cos\theta$$

$$+\frac{1}{\rho}\left(\mu\nabla_p^2 u_\theta + \frac{1}{a^2}\frac{\partial\mu}{\partial\theta}\frac{\partial u_\theta}{\partial\theta} + \frac{1}{a^2\sin^2\theta}\frac{\partial\mu}{\partial\varphi}\frac{\partial u_\theta}{\partial\varphi}\right)$$

$$+g\frac{\partial}{\partial p}\left(\mu\rho g\frac{\partial u_\theta}{\partial p}\right), \tag{A1}$$

$$\frac{\partial u_\varphi}{\partial t} = -\left(u_\theta \frac{1}{a}\frac{\partial u_\varphi}{\partial\theta} + u_\varphi \frac{1}{a\cdot\sin\theta}\frac{\partial u_\varphi}{\partial\varphi} + w\frac{\partial u_\varphi}{\partial p}\right) - \left(\frac{wu_\varphi}{a} + \frac{u_\theta u_\varphi}{a\cdot\tan\theta}\right)$$

$$-\frac{g}{a\cdot\sin\theta}\frac{\partial h_p}{\partial\varphi} - 2\Omega u_\theta \cos\theta$$

$$+\frac{1}{\rho}\left(\mu\nabla_p^2 u_\varphi + \frac{1}{a^2}\frac{\partial\mu}{\partial\theta}\frac{\partial u_\varphi}{\partial\theta} + \frac{1}{a^2\sin^2\theta}\frac{\partial\mu}{\partial\varphi}\frac{\partial u_\varphi}{\partial\varphi}\right)$$

$$+g\frac{\partial}{\partial p}\left(\mu\rho g\frac{\partial u_\varphi}{\partial p}\right). \tag{A2}$$

Here u_θ and u_φ are the neutral wind components, defined as positive southward and eastward, respectively; a is the distance to the center of the planet, θ is colatitude, φ is the longitude, h_p is the height of the pressure level, and t is time. Furthermore, g is the (height-dependent) gravitational acceleration, ρ is the mass density, p is the pressure, Ω is Titan's rotation period (with $\Omega = 4.6 \times 10^{-6}$ s^{-1}, corresponding to 15.8 Earth days), and μ is the coefficient of viscosity. Here w is the vertical wind in the pressure frame, defined as $w = dp/dt$. The total vertical velocity in the height frame u_z is obtained by adding the the velocity of the pressure level itself to the velocity relative to the pressure level, $-1/(\rho g)\, w$: $u_z = (\partial h_p/\partial t) - 1/(\rho g)\, w$.

[47] $\vec\nabla_p$ is the two-dimensional gradient operator on a level of fixed pressure. For its square we use the expression

$$\nabla_p^2 = \frac{1}{a^2}\frac{\partial^2}{\partial\theta^2} + \frac{\cos\theta}{a^2\sin\theta}\frac{\partial}{\partial\theta} + \frac{1}{a^2\sin^2\theta}\frac{\partial^2}{\partial\varphi^2}. \tag{A3}$$

In the vertical direction, the pressure gradient and gravity acceleration dominate other terms by several orders of magnitude and an accurate numerical calculation of the vertical velocity w by solving the vertical component of the momentum equation is numerically difficult. Vertical winds are therefore calculated using the continuity equation which in the pressure coordinate system reduces to the simple form of

$$\frac{1}{a\cdot\sin\theta}\frac{\partial}{\partial\theta}u_\theta\sin\theta + \frac{1}{a\cdot\sin\theta}\frac{\partial u_\varphi}{\partial\varphi} + \frac{\partial w}{\partial p} = 0. \tag{A4}$$

Physically, the equation expresses that any divergence in the horizontal velocity field must be balanced by vertical wind in order to conserve mass. To calculate w we use the technique described by *Müller-Wodarg et al.* [2000]. As boundary conditions for the momentum equation we assume fixed wind velocities (of zero) at the bottom and vanishing vertical gradients of wind components at the top level.

[48] The energy balance is given by the sum of the internal and external energy sources and sinks. In a spherical pressure coordinate system it may be expressed by the relation

$$\frac{\partial \epsilon}{\partial t} + \vec{U}_p \cdot \vec{\nabla}_p(\epsilon + gh_p) + w\frac{\partial(\epsilon + gh_p)}{\partial p} = Q_{EUV} + Q_{IR}$$
$$+ g\frac{\partial}{\partial p}\left(\frac{(K_m + K_\tau)}{H}p\frac{\partial T}{\partial p}\right) + \frac{1}{\rho}(K_m + K_\tau)\nabla_p^2 T$$
$$+ g\frac{\partial}{\partial p}\left(u_\theta\mu\frac{\partial u_\theta}{\partial p} + u_\varphi\mu\frac{\partial u_\varphi}{\partial p}\right). \quad (A5)$$

Here ϵ is the sum of internal and kinetic energies per unit mass, defined as $\epsilon = c_p T + 0.5\ (u_\theta^2 + u_\varphi^2)$, and T is gas temperature. With gh_p representing the potential energy of the gas at height h_p, the term $\epsilon + gh_p$ is thus its enthalpy. K_m and K_τ are coefficients of molecular and turbulent conduction, respectively. The principal external energy source in Titan's atmosphere Q_{EUV} is solar EUV and FUV radiation which is absorbed by CH_4 and N_2 at wavelengths between 75 and around 1300 Å, in particular the Lyman α (1216 Å) and He II (304 Å) lines. Radiative cooling Q_{IR} in Titan's thermosphere occurs via the rotational bands of HCN. In the model we calculate the HCN IR cooling self-consistently, taking into account radiative transfer. We currently assume only solar EUV and FUV heating and ignore possible further energy influx from above (precipitating particles from Saturn's magnetosphere) and below (upward propagating waves). As boundary conditions for the energy equation we assume fixed temperature (of 140 K) at the bottom and zero vertical temperature gradients at the top.

[49] In addition, our TGCM allows for the dynamical redistribution of individual gases by explicitly calculating their transport by winds and molecular and eddy diffusion. While transport by winds is treated both horizontally and vertically, we calculate molecular and eddy diffusion only in the vertical direction, since vertical gradients are much larger than horizontal gradients. The molecular diffusion velocities are given by

$$\frac{\partial Y_i}{\partial z} - \left(1 - \frac{m_i}{m} - \frac{H}{m}\frac{\partial m}{\partial z}\right)\frac{Y_i}{H} = -\sum_{j \neq i}\frac{mY_iY_j}{m_jD_{ij}}\left(w_i^D - w_j^D\right) \quad (A6)$$

where $Y_i = \rho_i/\rho$ and m_i are the mass fraction and molecular mass of the ith constituent, respectively, m is the mean molecular mass of the atmosphere, H is the pressure scale height, D_{ij} is the binary diffusion coefficient, and w_i^D is the vertical diffusion velocity of the ith constituent [*Chapman and Cowling*, 1970]. Molecular constituents are also subject to eddy diffusion, which we calculate with

$$w_i^K = -K\frac{\partial \ln(Y_i)}{\partial z} \quad (A7)$$

where K is the eddy diffusion coefficient. Here, K represets mixing due to small-scale motions not resolved by the TGCM. The diffusion velocities are then used in the continuity equation to calculate the time development of mass fractions. The continuity equation for the ith constituent is given in spherical pressure coordinates by

$$\frac{\partial Y_i}{\partial t} + u_\theta\frac{1}{a}\frac{\partial Y_i}{\partial\theta} + u_\varphi\frac{1}{a\cdot\sin\theta}\frac{\partial Y_i}{\partial\varphi} + w\frac{\partial Y_i}{\partial p} = g\frac{\partial}{\partial p}\left(\rho Y_i\left(w_i^D + w_i^K\right)\right) + J_i$$
$$(A8)$$

where J_i is the net chemical source rate [*Dickinson and Ridley*, 1975]. The velocities u_θ, u_φ and w represent the mean velocity of the atmosphere, defined as the average of the velocities of individual constituents, and weighted by their mass densities.

[50] Our TGCM calculations include the three thermally active species in Titan's thermosphere, N_2, CH_4, and HCN. N_2 and CH_4 are treated as inert because the time constant for loss through photolysis is much longer than the diffusion time constant. While calculating individual diffusion velocities for each gas using equations (A6) to (A8), we assume equal temperatures for all. The density profiles for these constituents are determined by advective and diffusive processes in the thermosphere, assuming as boundary condition zero vertical fluxes at the top boundary. The HCN density is modeled by specifying an empirical daytime production rate in the thermosphere and requiring $w_{HCN}^K = -K/H$ at the lower boundary. We assume a Gaussian distribution of the HCN production, which is centered around 850 km altitude, using a height-integrated production rate of 1×10^9 cm^{-2}s^{-1}, consistent with studies by *Fox and Yelle* [1997]. For CH_4 we assume a constant number mixing ratio of 1.7% at the bottom boundary.

[51] Molecular diffusion coefficients, in cgs units, are calculated with the formula $D = A(p_0/p)(T/T_0)^s$, where $p_0 = 0.147$ µbar, $T_0 = 135° K$, and A (s) for pairs CH_4-HCN, N_2-HCN and N_2-CH_4 are given by 3.64×10^5 (1.749), 2.12×10^5 (2.012), and 3.64×10^5 (1.749), respectively. We adopt an eddy coefficient for small scale motions of K = 5×10^7cm^{2}s^{-1}, assumed constant with altitude.

[52] Our present calculations use spatial resolutions of 6° latitude by 10° longitude by 0.25 scale heights vertically and integrate with a 20 s time step. Each simulation is run to steady state, which normally requires 16 Titan days. Further details of the model are given by *Müller-Wodarg et al.* [2000] and *Müller-Wodarg and Yelle* [2002].

References

Bougher, S. W., S. Engel, R. G. Roble, and B. Foster, Comparative terrestrial planet thermospheres: 2. Solar cycle variation of global structure and winds at equinox, *J. Geophys. Res.*, *104*, 16,591–16,611, 1999.

Chapman, S., and T. G. Cowling, *The Mathematical Theory of Non-Uniform Gases*, Cambridge Univ. Press, New York, 1970.

Dickinson, R. E., and E. C. Ridley, A numerical model for the dynamics and composition of the Venusian thermosphere, *J. Atmos. Sci.*, *32*, 1219, 1975.

Fox, J. L., and R. V. Yelle, Hydrocarbon ions in the ionosphere of Titan, *Geophys. Res. Lett.*, 24, 2179–2182, 1997.

Lebonnois, S., D. Toublanc, F. Hourdin, and P. Rannou, Seasonal variations of Titan's atmospheric composition, *Icarus*, 152, 384–406, 2001.

Lebonnois, S., F. Hourdin, P. Rannou, D. Luz, and D. Toublanc, Impact of the seasonal variations of composition on the temperature field of Titan's stratosphere, *Icarus*, 163, 164–174, 2003.

Müller-Wodarg, I. C. F., and R. V. Yelle, The effect of dynamics on the composition of Titan's upper atmosphere, *Geophys. Res. Lett.*, 29(23), 2139, doi:10.1029/2002GL016100, 2002.

Müller-Wodarg, I. C. F., R. V. Yelle, M. Mendillo, L. A. Young, and A. D. Aylward, The thermosphere of Titan simulated by a global three-dimensional time-dependent model, *J. Geophys. Res.*, 105, 20,833–20,856, 2000.

Rishbeth, H., and I. C. F. Müller-Wodarg, Vertical circulation and thermospheric composition: A modelling study, *Ann. Geophys.*, 17, 794–805, 1999.

Rishbeth, H., R. V. Yelle, and M. Mendillo, Dynamics of Titan's thermosphere, *Planet. Space Sci.*, 48, 51–58, 2000.

Strobel, F. D., M. E. Summers, and X. Zhu, Titan's upper atmosphere: Structure and ultraviolet emmissions, *Icarus*, 100, 512–526, 1992.

————————————

A. D. Aylward, Atmospheric Physics Laboratory, Department of Physics and Astronomy, University College London, 67-73 Riding House Street, London W1W 7EJ, UK. (a.aylward@ucl.ac.uk)

M. J. Mendillo, Center for Space Physics, Boston University, 725 Commonwealth Avenue, Boston, MA 02215, USA. (mendillo@bu.edu)

I. C. F. Müller-Wodarg, Space and Atmospheric Physics Group, Imperial College, Prince Consort Road, London SW7 2BW, UK. (i.mueller-wodarg@imperial.ac.uk)

R. V. Yelle, Department of Planetary Sciences, University of Arizona, 1629 E. University Blvd., Tucson, AZ 85721-0092, USA. (yelle@lpl.arizona.edu)